

# Coarse-graining dynamics for convection-diffusion of colloids: Taylor dispersion

Jimaan Sané,<sup>1,2</sup> Johan T. Padding,<sup>3</sup> and Ard A. Louis<sup>1</sup>

<sup>1</sup>*Rudolf Peierls Centre for Theoretical Physics, 1 Keble Road, Oxford OX1 3NP, United Kingdom*

<sup>2</sup>*Department of Chemistry, Cambridge University,  
Lensfield Road, Cambridge CB2 1EW, United Kingdom*

<sup>3</sup>*Computational Biophysics, University of Twente,  
PO Box 217, 7500 AE, Enschede, The Netherlands*

(Dated: December 4, 2018)

By applying a hybrid Molecular dynamics and mesoscopic simulation technique, we study the classic convection-diffusion problem of Taylor dispersion for colloidal discs in confined flow. We carefully consider the time and length-scales of the underlying colloidal system. These are, by computational necessity, altered in the coarse-grained simulation method, but as long as this is carefully managed, the underlying physics can be correctly interpreted. We find that when the disc diameter becomes non-negligible compared to the diameter of the pipe, there are important corrections to the original Taylor picture. For example, the colloids can flow more rapidly than the underlying fluid, and their Taylor dispersion coefficient is decreased. The long-time tails in the velocity autocorrelation functions are altered by the Poiseuille flow. Some of the conclusions about coarse-graining the dynamics of colloidal suspensions are relevant for a wider range of complex fluids.

PACS numbers:

## I. INTRODUCTION

Progress in computer simulations of materials arises from two broad classes of innovation. The first is better algorithms, for example more efficient ways to calculate equations of motion (for molecular dynamics) or to sample phase-space (for Monte Carlo). The second comes from better coarse-grained models of the underlying materials, that is descriptions that are simpler and more tractable, but nevertheless retain the fundamental underlying physics that one is interested in investigating. Of course progress also arises simply because computers are continually getting faster, so even with old models and old methods, new questions can become accessible.

The focus of this paper will be on new coarse-graining methods, especially for non-equilibrium properties of colloidal suspensions. That coarse-graining is needed becomes immediately obvious when considering the enormous *time* and *length-scale* differences between mesoscopic colloidal and microscopic solvent molecules. Even a nano-colloid of only 10 nm in radius will displace on the order of 140,000 water molecules. Moreover, such a small colloid would still need about  $5 \times 10^{-6}$  s to diffuse over its radius, while a typical collision time of water molecules is on the order of  $10^{-15}$  s. Simulating just a few nano-colloids in solution is therefore prohibitively expensive with any explicit model of water. On the other hand, it is clear from experiments that many general properties of colloidal suspensions, such as phase behaviour and basic non-equilibrium behaviour, do not depend strongly on the radius  $R$  of the particles, even though the number of water molecules per colloid scales as  $R^3$ . This physical fact immediately suggests that coarse-graining methods which ignore the fine detail of the solvent should be applicable.

A very fruitful coarse-graining strategy has been to

employ effective potentials that integrate out the solvent, and also other degrees of freedom, to create an intuitively appealing picture of colloids as “giant atoms” [1, 2]. Besides rationalising many results for equilibrium colloids, this viewpoint has stimulated the use of colloidal systems as a “playground” for probing some of the fundamentals of condensed matter physics. Colloids have the advantage that they are much larger than atoms, so that they are much more easily visualised. At the same time their length-scales are much longer, so that processes in the time-domain can be more easily investigated. Examples of what can be studied include the kinetics of crystallisation [3], the dynamics of supercooled liquids [4], glass formation [5, 6] interfacial phenomena [7], dislocation motion [8] and surface melting [9].

General processes in atomic and molecular materials where the non-equilibrium behaviour is dominated by the crossing of potential barriers, such as nucleation, glass formation and dislocation motion in crystals, are similar to the concomitant processes in colloidal systems. But at lower colloidal densities, it becomes less obvious that this should be the case. This is mainly because, in contrast to atoms, the colloids are in a solvent which induces Brownian motion and long-ranged hydrodynamic interactions (HI) [10, 11]. These HI may decay as slowly as  $1/r$  and can qualitatively affect the dynamical behaviour of a suspension. The question of how to coarse-grain away the solvent in such a way as to retain both the Brownian fluctuations and the long-ranged hydrodynamic interactions is a difficult one. In a previous paper [12] (henceforth paper I) we presented a careful analysis of how to achieve this using the stochastic rotation dynamics (SRD) algorithm of Malevanets and Kapral [13, 14]. Note that in the literature, this method is sometimes also called multiparticle collision dynamics, see the recent review by Kapral [15]. SRD has been applied to a

wide number of different systems, including fluid vesicles in shear flow[16], clay-like colloids[17], sedimentation of colloids[18, 19] colloidal rods in shear flow[20], knots in viral DNA[21] and other examples[15].

In the first section of this paper, we briefly review the method, and show how it can be used to bridge the time and length scales of a colloidal system where HI are important. A number of the lessons learned should be valid for other coarse-grained studies of dynamics. For example, we argue that many methods effectively use a “telescoping down” procedure to compress the physical time-scales to a more computationally manageable hierarchy. Once the simulations are completed, this hierarchy must be “telescoped out” in order to make contact with physical reality. Of course this cannot be done without losing some information; there is no such thing as a free lunch.

To further illustrate how such a coarse-graining method for dynamics can be used to investigate the combined effects of Brownian motion and HI on colloids, we study the diffusive behaviour of colloidal discs confined to a narrow two dimensional channels with a fluid undergoing Poiseuille flow. This convection-diffusion problem was first studied in a classic paper by G.I. Taylor [22]. He pointed out that if a solute diffuses between the streamlines of a flow field, this adds an axial diffusive component relative to the average flow field, an effect now called Taylor dispersion. In his original work, Taylor derived the asymptotic form of the dispersion coefficient. Van den Broeck [23] later derived an exact expression for the dispersion valid at all times. Rather surprisingly Taylor found that the effective spreading constant, or Taylor diffusion coefficient as we shall refer to it, was inversely proportional to the molecular diffusion coefficient  $D$  and has the form

$$D^* = \frac{\bar{u}^2 L^2}{48D} \quad (1)$$

where  $L$  denotes the channel radius and  $\bar{u}$  the average flow velocity for a three-dimensional pipe. Further work in the field has led to the development of a more generalised Taylor dispersion theory, as illustrated in the review by Van den Broeck [24]. Dispersion theory can have applications in a multitude of disciplines. Oscillatory flows, such as those that arise in estuaries and blood flow have been the subject of intensive study [24]. The effect of interparticle interactions, such as chemical reactions and different boundary conditions are also of interest [24]. Much of this work has focussed on particles whose radius  $R$  is much smaller than the channel radius  $a$ . Here we study in particular what happens to Taylor dispersion and related problems when the colloidal radius is no longer negligible compared to the pipe radius, building on earlier work by Brenner and Edwards[25]. In such situations, we find that the colloid flows faster than the average of the underlying solvent, mainly because the colloid can only sample the faster flow lines near the centre of the flow profile. At the same time, the Taylor dispersion coefficient is decreased, because the colloid can

sample a smaller range of flow velocities. For very narrow pipes more subtle hydrodynamic effects due to direct interactions with the walls start to become important.

The paper is organised as follows: In section II we discuss some salient points of our coarse-graining scheme for colloids. In section III we describe Taylor dispersion for point particles, whereas section IV considers the case where the colloid radius is no longer negligible compared to the pipe width. Finally, in section IV, we summarise our main conclusions.

## II. COARSE-GRAINING COLLOIDAL DISPERSIONS

### A. Effective potentials for colloids

The detailed interactions between colloidal particles can be very complex and affected by other (smaller) colloidal particles, polymers, ions and the properties of the underlying solvent. However, much progress can be made by integrating out these degrees of freedom to generate an effective picture with radial potentials[1, 2]. The advantage of these are that the well-developed statistical mechanical machinery developed for atomic and molecular potentials can now be applied to colloidal suspensions. Of course colloids can also be more complicated, for example much recent progress has been made on “colloidal molecules”[26], and colloids can easily have anisotropic interactions[27]. But even for these systems, the picture of effective potentials is a powerful abstraction[28].

Nevertheless, it must always be kept in mind that these effective potentials are not potential energy functions in the Hamiltonian sense, but rather include within their definition statistical averages over configurations. Their character is therefore that of a free-energy. This has a number of implications such as *transferability problems*, where a potential derived in one context does not perform well in another context. A good example would be if the derived potential depends on the overall colloid density. Then using it at a different density could lead to errors.

Another, more subtle, but perhaps equally important issue is that of *representability problems*[29], where the effective potential may be used to represent a certain subset of physical quantities, but not a different subset.

For example, consider a one-component colloidal fluid interacting with a three-body Hamiltonian of the form:

$$H = K + \sum_{i < j} w^{(2)}(r_{ij}) + \sum_{i < j < k} w^{(3)}(\mathbf{r}_{ij}, \mathbf{r}_{jk}, \mathbf{r}_{ki}), \quad (2)$$

where  $\mathbf{r}_i$  denotes the position of particle  $i$  and  $\mathbf{r}_{ij} = \mathbf{r}_i - \mathbf{r}_j$  and  $r_{ij} = |\mathbf{r}_i - \mathbf{r}_j|$ .  $K$  is the kinetic energy operator,  $w^{(2)}(r)$  is an isotropic pairwise additive potential, and  $w^{(3)}(\mathbf{r}_{ij}, \mathbf{r}_{jk}, \mathbf{r}_{ki})$  is a triplet or three-body potential. Three-body potentials are expensive and cumbersome to simulate, and so one might want to coarse-grain them to a simpler isotropic pair representation.

Henderson [30] first showed, using arguments very similar to those used by Hohenberg and Kohn [31] in their famous proof relating the one-body potential to the one-body density (which laid the foundation for density functional theory), that “the pair potential  $v(r)$  which gives rise to a radial distribution function  $g(r)$  is unique up to a constant.”. An extended proof for orientational correlations can be found in a book by Gray and Gubbins [32], while a more rigorous mathematical discussion is provided by Chayes, Chayes and Lieb [33]. This means that, for a given state-point, the  $g(r)$  generated by a Hamiltonian like that of Eq. (2) can be reproduced by a unique effective pair potential  $v_g(r)$ . We call approaches that derive  $v_g(r)$  the structural route to deriving an effective potential. The difference with the bare-pair potential  $w^{(2)}(r)$  can be written as:

$$\delta v_g(r) = w^{(2)}(r) - v_g(r). \quad (3)$$

Similarly, one could derive an effective potential via an energy route, such that the full internal energy of a system at a state point  $(N, V, T)$ , governed by the Hamiltonian (2), is reproduced by the simpler two-body formula

$$U(N, V, T) = \frac{1}{2} \rho^2 \int d\mathbf{r}_1 d\mathbf{r}_2 g(r_{12}) v_U(r_{12}). \quad (4)$$

The difference with the bare-pair potential  $w^{(2)}(r)$  can be written as:

$$\delta v_U(r) = w^{(2)}(r) - v_U(r). \quad (5)$$

It is not hard to show that both  $v_g(r)$  and  $v_U(r)$  depend on the state point at which they are derived. Thus if they are used at a different state-point, one would expect transferability problems. What is perhaps more worrying is that one can also show that at a given state-point,  $v_g(r)$  and  $v_U(r)$  cannot be the same. For example, To lowest order in  $\rho$  and  $w^{(3)}$ , the ratio between the two corrections is [29, 34, 35]:

$$\frac{\delta v_U(r)}{\delta v_g(r)} = \frac{1}{3} + \mathcal{O}\left((w^{(3)})^2; \rho^2\right). \quad (6)$$

Since  $v_g(r)$  is unique, it is therefore impossible to represent the properties of a system governed by the Hamiltonian of Eq. (2) by a single pair potential. These *representability problems* are widespread in coarse-grained descriptions of soft-matter systems[29]. They are also important in other coarse-grained simulations. For example, one of us recently studied the structural route to derive radially symmetric potentials for water[36]. There  $v_g(r)$  and  $v_U(r)$  were explicitly constructed and look very different, as anticipated by Eq. 6). At some relevant state-points, using  $v_g(r)$  to calculate the virial pressure resulted in a compressibility factor  $Z$  that was almost two orders of magnitude larger than that of the original multi-site water model used to parameterise  $v_g(r)$ . Admittedly, it may not be surprising that an isotropic

potential should perform so poorly when the underlying fluid has complex orientational correlations. On the other hand, one could derive a potential  $v_P(r)$ , designed to correctly predict the virial pressure of the underlying water model. But, due to the uniqueness of  $v_g(r)$ , this potential would no longer correctly reproduce the pair correlations. It is really a case of “choose your poison”.

In practice, things may not always be so dire for many colloidal suspensions. First of all, one is not usually trying to reproduce all properties as accurately as one needs to for a molecular fluid like water. Secondly, for many hard-core colloids with short-ranged interactions, the state-dependence of the interactions is not expected to be too important. In this case, transferability and representability problems, which are often linked[29], are not expected to be strong.

For more complex soft-matter systems the story is more subtle, see e.g. a paper by Murtola *et al.*[37] for an excellent discussion for the case of lipid bilayers. In general, careful coarse-graining often leads to potentials that are much softer than normal atomic or molecular fluids [1, 2, 38, 39]. This can have important advantages when performing equilibrium calculations, because energy barriers are lowered, making, for example, Monte Carlo sampling more efficient. When used in dynamical simulations, however, the correct application of effective potentials is more difficult to properly derive. For example, in the “polymers as soft-colloids” picture[38], the inter-polymer interactions are so soft that polymers can easily pass through one another. This is clearly not physical, and so schemes that use effective potentials for polymer dynamics must re-introduce crossability constraints to prevent coarse-grained polymers from passing through one another [40]. Depletion interactions in a multi component solution also depend on the relative rates of depletant diffusion coefficients and particle flow velocities [41, 42]. Thus care must be taken that the components integrated out can respond much more rapidly than the colloids move, so that an effective potential picture still approximately holds.

In this context it is illuminating to consider the statistical mechanical origins of dissipative particle dynamics (DPD), which also relies on soft interactions[43, 44]. As discussed in paper I, this method includes two separate innovations. The first is to use soft-potentials. As described above, these can indeed be very useful for speeding up sampling of equilibrium behaviour. For non-equilibrium behaviour however, the application of these potentials remains somewhat obscure. One hopes that the significant lowering of energy barriers leads nonetheless to relative time-scales that are qualitatively correct. If this can indeed be shown to be the case, then the soft potentials are a very useful computational tool. In practice however, this is often hard to show with any certainty, which often limits the reliability or physical relevance of many DPD simulations.

The second independent innovation in DPD arises from the use of a thermostat that conserves momentum.

Molecular dynamics simulations are most naturally performed in the microcanonical ensemble, but most investigators prefer to use other ensembles such as the canonical ensemble. To achieve this, they implement a thermostat. The problem is that many thermostats don't exactly conserve momentum, and so the hydrodynamic interactions that would naturally be present in the microcanonical calculations are not rendered correctly. The DPD thermostat solves this problem. However, it can also be used with other inter-particle interactions, and doesn't depend on innovation 1 of DPD, the use of soft potentials.

For colloids in solution however, using the DPD thermostat does not generate the correct hydrodynamics without a complete simulation of the underlying solvent. As pointed out before, this is highly inefficient, and so a different approach must be used, and that will be the subject of the next section.

### B. Coarse-graining dynamics of colloids

To describe the dynamics of colloidal suspensions, we follow paper I and implement the SRD method first derived by Malevanets and Kapral [13]. The method works by exploiting the fact that Navier Stokes hydrodynamics arises from local momentum conservation. Thus one can employ greatly simplified dynamics that are computationally very efficient to simulate, and still generate hydrodynamic behaviour. There are many methods in this class, including direct simulation Monte Carlo (DSMC) method of Bird [45, 46] and the Lattice Boltzmann (LB) technique where a linearized and pre-averaged Boltzmann equation is discretised and solved on a lattice [47]. In particular Ladd and others have extended this method to model colloidal suspensions [48, 49, 50, 51, 52, 53]. SRD has the particular advantage that transport coefficients have been analytically calculated [54, 55, 56], greatly facilitating its use. It is important to remember that for all these particle based methods, the particles should not be viewed as some kind of composite supramolecular fluid units, but rather as coarse-grained Navier Stokes solvers (with noise in the case of SRD) [12].

The SRD fluid is modelled by  $N$  point particles of mass  $m$ , with positions  $\mathbf{r}_i$  and velocities  $\mathbf{v}_i$ . The coarse graining procedure consists of two steps, streaming and collision. During the streaming step, the positions of the fluid particles are updated via

$$\mathbf{r}_i(t + \delta t_c) = \mathbf{r}_i(t) + \mathbf{v}_i(t)\delta t_c. \quad (7)$$

In the collision step, the particles are split up into cells with sides of length  $a_0$ , and their velocities are rotated around an angle  $\alpha$  with respect to the cell centre of mass velocity,

$$\mathbf{v}_i(t + \delta t_c) = \mathbf{v}_{c.m,i}(t) + \mathcal{R}_i(\alpha) [\mathbf{v}_i(t) - \mathbf{v}_{c.m,i}(t)] \quad (8)$$

where  $\mathbf{v}_{c.m,i} = \sum_j^{i,t} (m\mathbf{v}_j) / \sum_j m$  is the centre of mass velocity of the particles the cell to which  $i$  belongs,  $\mathcal{R}_i(\alpha)$

is the cell rotational matrix and  $\delta t_c$  is the interval between collisions. The purpose of this collision step is to transfer momentum between the fluid particles while conserving the energy and momentum of each cell. The algorithm is efficient because direct interactions between the particles are not taken into account.

Spherical colloids of mass  $M$  can be embedded in an SRD solvent using a Molecular Dynamics technique, as first shown by Malevanets and Kapral [14], and studied in detail in reference I. We employ the following scheme: For the colloid-colloid interaction we use a standard steeply repulsive potential of the form:

$$\varphi_{cc}(r) = \begin{cases} 4\epsilon \left( \left( \frac{\sigma_{cc}}{r} \right)^{48} - \left( \frac{\sigma_{cc}}{r} \right)^{12} + \frac{1}{4} \right) & (r \leq 2^{1/24}\sigma_{cc}) \\ 0 & (r \geq 2^{1/24}\sigma_{cc}) \end{cases}$$

while the interaction between the colloid and the solvent is described by a similar, but less steep, potential:

$$\varphi_{cs}(r) = \begin{cases} 4\epsilon \left( \left( \frac{\sigma_{cs}}{r} \right)^{12} - \left( \frac{\sigma_{cs}}{r} \right)^6 + \frac{1}{4} \right) & (r \leq 2^{1/6}\sigma_{cs}) \\ 0 & (r \geq 2^{1/6}\sigma_{cs}) \end{cases}$$

where  $\sigma_{cc}$  and  $\sigma_{cs}$  are the colloid-colloid and colloid-solvent collision diameters. We propagate the ensuing equations of motion with a Velocity Verlet algorithm using a molecular dynamic time step  $\Delta t$

$$R_i(t + \Delta t) = R_i(t) + V_i(t)\Delta t + \frac{F_i(t)}{2M}\Delta t^2 \quad (9)$$

$$V_i(t + \Delta t) = V_i(t) + \frac{F_i(t) + F_i(t + \Delta t)}{2M}\Delta t \quad (10)$$

where  $R_i$  and  $V_i$  are the position and velocity of the colloid, and  $F_i$  the total force exerted on the colloid. Coupling the colloids in this way leads to slip boundary conditions. Stick boundary conditions can also be implemented [57], but for qualitative behaviour, we don't expect there to be important differences. In parallel the velocities and positions of the SRD particles are streamed in the external potential given by the colloids and the external walls and updated with the SRD rotation-collision step every time-step  $\delta t_c$ . We chose  $\sigma_{cc} = 4.3a_0$ . The choice of time-steps, as well as a number of other technical issues are described in more detail in ref I, and for the case of two-dimensional discs, in [58].

One key step in the implementation and interpretation of these kinds of coarse-grained dynamical simulations lies in the realisation that hydrodynamic phenomena depend primarily on a set of dimensionless numbers, and that it is important to keep these in the right regimes in order to simulate the correct physical behaviour. Typical numbers include the Reynolds number  $Re$  which measures the relative strength of viscous and inertial forces, and the Mach number  $Ma$ , defined as the ratio of a typical colloidal velocity to the velocity of sound  $c_s$  of the underlying fluid. In a real colloidal system, the  $Re$  and  $Ma$  numbers are very small, typically on the order of  $10^{-6}$  or less. However, as long as one keeps them less than about

$10^{-1}$ , the physical regime doesn't really change much, a fact that can be exploited in simulations. For example if the real Ma number of a colloidal suspension were reproduced, it would mean that millions of sound waves would need to be resolved for modest motion of the colloids. But to be in the right physical regime, a sound velocity well separated from other velocities is all that is needed. Obviously having a slower sound speed greatly increases the efficiency of the simulation. The example of the Ma number can be extended to a whole range of other hydrodynamic numbers, as discussed in more detail in reference I[12].

A related set of arguments can be made for the time-scales of a typical colloidal system. A colloid of radius  $1\mu m$  diffuses over its radius in a time of order several seconds. At the same time, the shortest physically relevant time-scale for the colloidal dynamics is the Fokker-Planck time  $\tau_{FP}$ , defined in [11] as the time over which the colloidal force-force correlation function decays. For a typical colloid, this may be as small as  $10^{-13}s$ . Other important time-scales include the sonic time-scale  $t_{cs} = R/c_s$ , on the order of  $10^{-10}s$  for a typical colloid. The kinematic time-scale  $\tau_\nu = R^2/\nu$  which measures the time for vorticity, which diffuses with the kinematic viscosity  $\nu$ , to diffuse over one colloidal radius is also important, and linked to the Re number. In a real colloidal system, these time-scales are all separated from each other by many orders of magnitude. However, to be in the correct physical regime, one doesn't necessarily need to resolve all those time-scales. All that is really needed is a clear time-scale separation.

Our strategy is then as follows: First, the relevant time-scales are identified. These are then *telescoped* down to a hierarchy which is compacted to maximise simulation efficiency, but sufficiently separated to correctly resolve the underlying physical behaviour. We illustrate this process in Figure 1, and discuss it in more detail in ref I. Although the particular example studied here concerns a colloid in suspension, we argue that many other coarse-graining methods make implicit use of some aspect of telescoping down. A careful time-scale analysis is very important for the correct physical interpretation of the simulation results.

Having sketched our simulation technique, we now turn to an application where diffusion, convection, and hydrodynamic interactions all play a role.

### III. TAYLOR DISPERSION FOR SMALL SOLUTES

When a fluid flows between two parallel plates, stick boundary conditions mean that the local fluid velocity is zero at the plate surfaces. The resulting Poiseuille flow has a velocity distribution of the form [59]:

$$u(y) = \frac{3}{2}\bar{u}\left(1 - \frac{y^2}{L^2}\right), \quad (11)$$

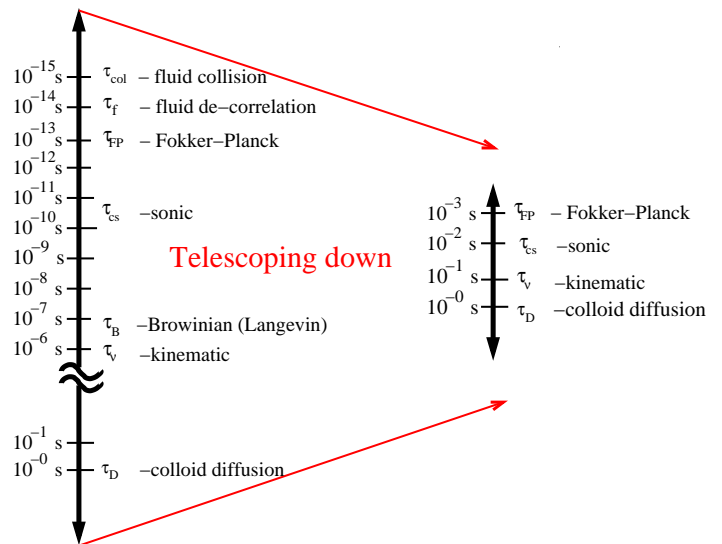


FIG. 1: Telescoping down: The hierarchy of time-scales for a colloid (here the example taken is for a colloid of radius  $1\mu m$  in  $H_2O$ ) is compressed in the coarse-grained simulations to a more manageable separation. As long as the physically important times are clearly separated, the simulation should still generate the correct physical picture. Once the simulations are completed, they can be related in more detail to particular experiments by telescoping back out to the relevant experimental time-scales.

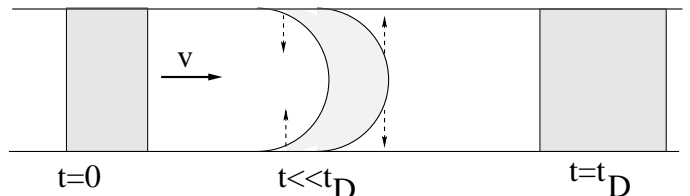


FIG. 2: Taylor dispersion between parallel plates. The initial solute gets stretched to a paraboloid shaped plug. Diffusion, indicated by the vertical arrows, evens out the concentration profile leading to a wider plug. Taylor dispersion describes the diffusive spreading of the plug.

where  $\bar{u}$  is the mean velocity,  $2L$  is the plate separation, and  $y$  is a coordinate measuring the distance from the centre of the pipe. Thus the maximum velocity  $u_0 = \frac{3}{2}\bar{u}$  is at the centre of the flow profile.

The basic idea behind Taylor dispersion is that a solute particle will diffuse between the streamlines. Its average position moves forward with the average flow velocity, but because some streamlines move faster than the average, and some slower, the diffusion between streamlines adds an extra dispersive component relative to its average motion in the axial direction.

To get a better physical understanding of Taylor diffusion, we follow an argument from [60], depicted in fig.2. For time scales less than  $t_D \sim L^2/D$ , convection initially stretches the solute into a parabola. The solute at the

front end of the parabola leads the solute at the edges by a distance  $u_0 t$  after a time  $t$ . Diffusion across the channel then smears the parabola into a plug in a time-scale  $t_D$  it takes the solute to reach the edges. Thus the parabola is smeared into a plug of width  $W_{tD} \sim u_0 t_D = u_0 L^2 / D$ . We can describe this as the the plug taking a random step of size  $\sim W_{tD}$  at each ‘step’  $t_D$ . If we now repeat the process for different stripes of the plug; each convectively stretched then diffusively smeared, then after  $N$  steps, the plug will have evolved as

$$\langle W^2 \rangle \sim N W_{tD} \sim \left( \frac{u_0^2 L^2}{D} t \right). \quad (12)$$

Accordingly, in addition to molecular diffusivity  $D$ , the solute can be seen to diffuse along the channel, with respect to the average flow, with an effective dispersion coefficient

$$D^* \sim \frac{u_0^2 L^2}{D}. \quad (13)$$

Note that the effective dispersion coefficient is inversely proportional to the molecular diffusion coefficient, which may seem counter intuitive at first glance. However, solute molecules with higher molecular diffusivities spend more time diffusing across the pipe and less time sampling particular velocity streamlines thus reducing their *effective* spreading.

A more sophisticated calculation based on flow in a three dimensional pipe of radius  $L$  yields a prefactor [61]

$$D^* = \frac{\bar{u}^2 L^2}{48D}. \quad (14)$$

In previous work [63] we have calculated the exact value for the prefactor in two dimensions. By integrating the equations of motion over the plate separation and implementing the appropriate boundary conditions we found that

$$D^* = \frac{2\bar{u}^2 L^2}{105D}. \quad (15)$$

In this paper we will carry out most of our simulations and analysis in two dimensions, simply because simulations are easier, and the fundamental physics we are after should not be very dependent on the exact dimension we work in.

The calculations above assume that the molecular diffusion in the axial direction is negligible. When this is not the case, a good approximation for the Taylor dispersion coefficient was first given by Aris [64] to be:

$$D_{TA} = D^* + D, \quad (16)$$

and so  $D_{TA}$  is often called the Taylor-Aris dispersion coefficient.

Taylor dispersion has been extensively used to study the diffusion coefficients of small molecular solutes[65] where  $D$  is typically  $10^{-8} \text{cm}^2/\text{s}$  so that  $D^*$  is expected

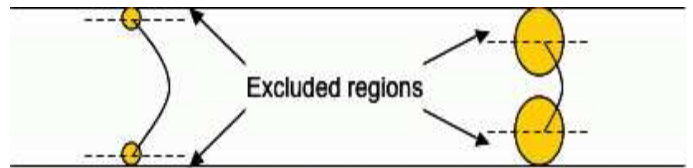


FIG. 3: Finite size effect correction to the flow profile. Colloids are no longer able to velocity gradients near the walls resulting in an average velocity higher than that of the solvent.

to be large, making it easy to measure. Experimental setups examining atomic Taylor dispersion use tubes of order a few *mm* in diameter and lengths many meters. In such setups,  $D$  can be measured with an accuracy of  $\pm 1\%$  [24]. For colloidal systems, where diffusion coefficients are much smaller, it may be possible to use a shorter tube, because the Taylor-Aris dispersion coefficient would in fact be much larger.

#### IV. TAYLOR DISPERSION OF FINITE SIZED COLLOIDAL DISCS

As illustrated in Fig. III, when the colloid radius becomes comparable to  $L$ , the colloids can no longer sample the entire Poiseuille flow profile. This leads to a number of corrections [25]. Firstly, because the colloids are excluded from the slower flow-lines, their average velocity is faster than the underlying flow of the fluid. This can easily be calculated for Poiseuille flow

$$u_c = \frac{3}{2} \frac{\bar{u}}{L-R} \int_0^{L-R} \left( 1 - \frac{y^2}{L^2} \right) dy = \frac{3}{2} \bar{u} \left( \frac{2}{3} + \frac{2}{3}\chi - \frac{1}{3}\chi^2 \right). \quad (17)$$

where  $\chi = R/L$  measures the size of the colloid compared to the distance between the plates. For infinitely small particles with  $\chi = 0$  the average velocity is  $u_c = \bar{u}$ , but as  $\chi$  increases, so does the average velocity, until it reaches a maximum of  $u_c = \frac{3}{2}\bar{u}$  at  $\chi = 1$ . This size exclusion phenomenon can be used to analyse the relative diameters of colloidal particles (hydrodynamic chromatography [66]).

For finite  $\chi$ , the Taylor dispersion coefficient also undergoes corrections[25]. If the new boundary conditions are taken into account, then our calculation of Eq.(15) incurs further corrections [63]:

$$D^* = \frac{\bar{u}^2 L^2}{D} \left( \frac{(1-\chi)^4}{30} - \frac{(1-\chi)^6}{70} \right) \quad (18)$$

for  $2d$  flows. The radial dispersion of the colloids is now effectively reduced as they are unable to sample the higher velocity gradients near the edges, reducing the radial dispersivity and leading to a lower value of the Taylor dispersion coefficient.

Note, however, that the calculations above assumed that **1**, the colloids perfectly follow the stream-lines, and are not themselves affected by their proximity to the

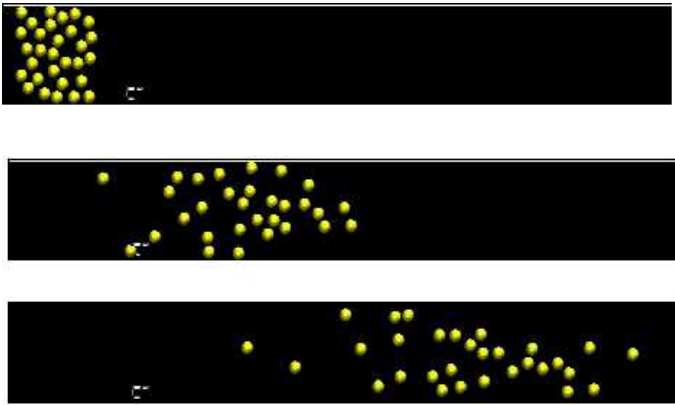


FIG. 4: Simulation snapshots at different time-intervals of the Taylor diffusion of colloids in a flow field.

plates, and **2**, that the average flow profile is not itself perturbed by the presence of the colloids. For three dimensions, Brenner & Gaydos [67] used a moment analysis to show that extra terms enter into Eq.(17) that reduce the numerical coefficients so that the actual flow velocity is lower than a calculation which ignores the wall effects. What happens to the average flow in two dimensions, and how this exactly affects the Taylor dispersion beyond that shown in Eq. (18), is not known.

To study the effect of finite particle size we performed computer simulations of colloids and heavier SRD tracer particles using the methodology described in papers I and [58]. Fig. IV shows some typical snapshots of colloidal dispersion driven by Taylor dispersion. We take care to make sure that the Re number is always less than about 0.1, and that other hydrodynamic numbers are also in the correct regime. We simulate with up to 60 colloids and for box lengths of  $238R$ . Averages are measured after the transients are deemed to have decayed away.

One effect that the colloids can have on the flow is that they increase the viscosity, which in turn affects the average velocity. This is shown in the top panel of Fig. 5. By fitting the measured profile for different colloid packing fractions  $\phi$  we find that the viscosity of the mixture scales roughly as  $\eta_\phi \sim (1 + 1.95\phi)\eta_0$ . In three dimensions and in the bulk, the pre-factor in front of  $\phi$  is 2.5 [10, 11].

In the bottom panel of Fig. 5 we show the average velocity of colloidal particles as a function of the radius to pipe-size ratio  $\chi$ . These show a decrease of their velocity compared to the ideal calculation of Eq. (17) due to the effect of hydrodynamic interactions with the walls. We also tested the average velocity of SRD tracer particles (“ideal colloids”). These have a larger mass than the other fluid point particles, and in addition, interact with the walls with an interaction of radius  $R$ . Otherwise they are point-particles and participate in the SRD collision rules. We expect that these particles have a smaller effect on the fluid flow profile than the colloids do. As shown in Fig. 5, these particles also don’t follow the ideal correction term, and so presumably also experience hy-

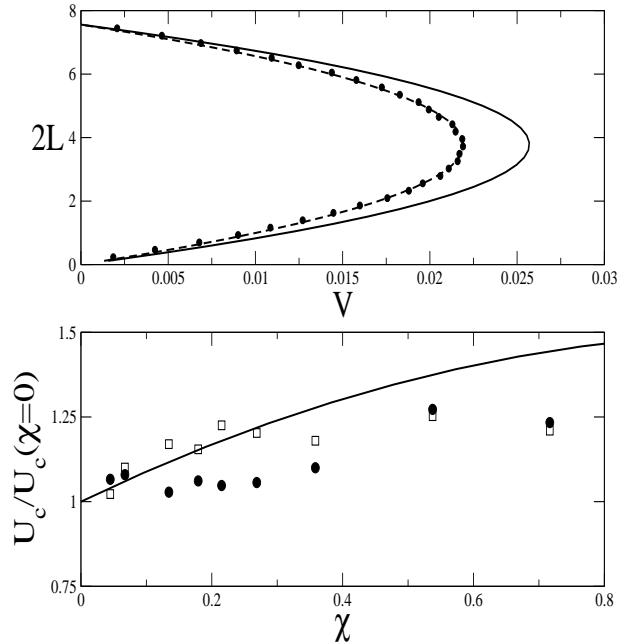


FIG. 5: Top : Effect of the colloid concentration on the solvent flow profile. The straight line represents the theoretical flow profile for a pure SRD solvent. The simulation points represent the flow profile for a homogeneous distribution of colloids at a packing fraction of  $\phi = 0.1$  while the dotted line shows the fit with the increased viscosity. Bottom : The average flow velocities of colloids (circles) and “ideal” colloids (squares) are compared to the original simple prediction of Eq. 17 that ignores the effects of the walls. As expected, for increasing  $\chi = R/L$ , the walls on average slow down the particles compared to what one would expect if they just followed the unperturbed Poiseuille flow lines.

drodynamic interactions with the wall that slow them down.

Within a simple Langevin picture, a colloid loses memory its velocity on a time-scale given by  $t_\xi = M/\xi$ , where the friction coefficient  $\xi$  is defined by  $D = k_B T/\xi$ . Although for colloids this Langevin picture is in fact heavily misleading, see e.g. the discussion in the appendix of ref I[12], for our purposes here it should suffice as a useful reference time-scale.

If the fluctuation-dissipation theorem is invoked, then an effective Taylor dispersion friction  $\xi^*$  can be defined, such that  $D^* = \frac{k_B T}{\xi^*}$ . In a simple Langevin picture, fluctuations will die out on the time scale

$$t_{\xi^*} = \frac{M}{\xi^*} = \frac{MD^*}{k_B T} = \frac{2}{105} \frac{MD \bar{u}^2 L^2}{k_B T D^2} = \frac{2}{105} t_\xi Pe^2 \quad (19)$$

where we have defined the pipe Peclet number

$$Pe = \frac{\bar{u}L}{D} = t_U / \tau_{DL} \quad (20)$$

which can be viewed as the ratio of the time  $t_U = L/\bar{u}$

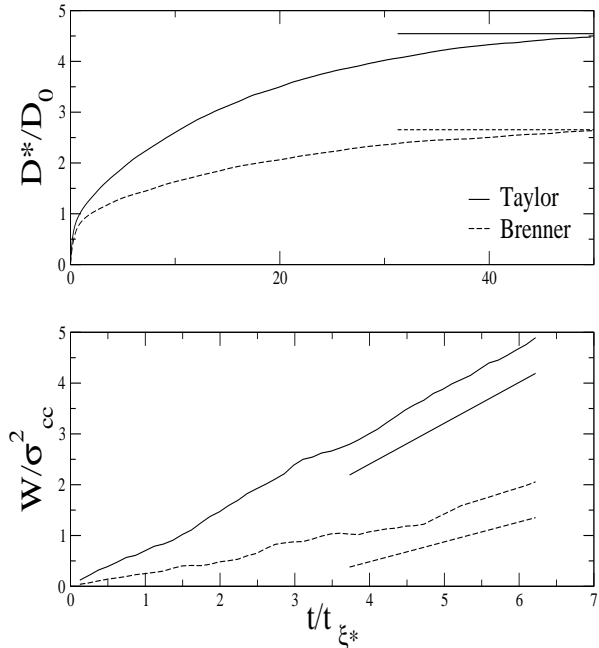


FIG. 6: Top panel: Integral of the velocity fluctuations. Bottom panel: Effective mean square displacement with respect to the average flow. Both graphs are for “ideal colloids” made up of heavier SRD particles.

it takes the fluid to move in the axial direction over a distance  $L$ , to the time  $\tau_{DL}$  it takes a particle to diffuse that distance.

To measure Taylor dispersion as accurately as possible, we simulated ‘ideal’ colloids of mass  $M = 62.3m$  under flow and measured the dispersion of 25 of these in a pipe of width such that  $\chi = 0.134$ . A separate set of simulations was done in the same pipe, but with “ideal” SRD colloids with the same wall-colloid interaction as the solvent. For these ideal particles and the relatively wide pipe, we don’t expect strong wall effects, so that the simple Eq. (18) should provide a good approximation to the Taylor dispersion. The results of these simulations are shown in Fig.6. The plain curves denote results for the heavier SRD fluid particles without an extra wall-interaction, while the dashed curves depict results for “ideal colloids”, i.e. the heavier SRD particles with an extra interaction with the wall. In the top section of the graph, we have plotted the integral of the velocity auto-correlation function for both sets of particles. The horizontal lines are a guide to the eye and intersect the  $y$ -abscissas at the theoretical values for dispersion predicted in Eq. (18) for  $\chi = 0$  and  $\chi = 0.134$  respectively. In both instances, we see that the simulated integrals plateau near the lines suggesting good agreement with Taylor theory, including the corrections of Eq. (18). The lower part of Fig.6 shows the mean squared displacement of the particles w.r.t. the average of the centre of mass of

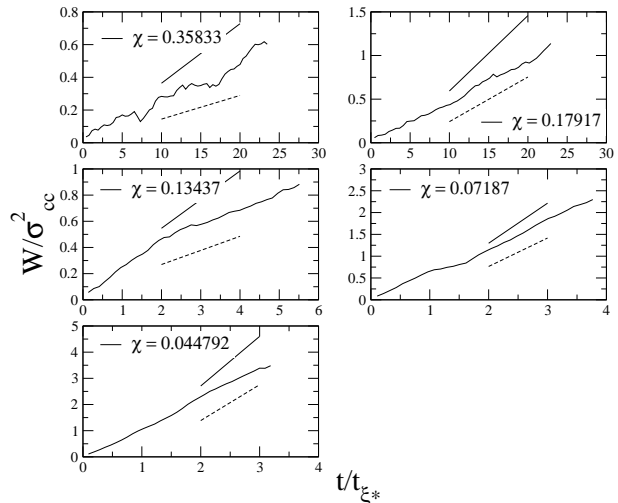


FIG. 7: Effective mean square displacement of colloids undergoing Taylor dispersion. Simulations were carried out in pipes of sizes  $\chi = 0.358, 0.179, 0.134, 0.0719, 0.0448$  respectively. The solid straight line represents the approximation for Taylor dispersion from Eq. (15), and the dotted lines denote the finite size correction predicted in Eq. (18). Simulation parameters were chosen to ensure that the self and Taylor dispersion are always clearly separated, i.e. that  $D^*/D = t_{\xi^*}/t_{\xi} \geq 5$ . All runs were carried out for colloid Reynolds number of less than 0.1.

a large number of colloids. This is expected to scale as  $X^2 \sim 2D^*t$ . Note that even for this relatively small value of  $\chi$ , the Taylor dispersion coefficient is down by about  $\frac{2}{3}$ , so that the effect of a finite size is much stronger on the Taylor dispersion than it is on the relative velocity of the particles, which only shows a very modest correction for that value of  $\chi$ .

Fig.7 depicts the mean square displacement w.r.t. the centre of mass flow of normal colloidal discs. The measured Taylor dispersion coefficient  $D^*$  appears to lie between the predictions of Eq. (15) and (18).

We also investigated the behaviour of the velocity autocorrelation function (VACF)  $C(t) = \langle \delta v(t) \delta v(0) \rangle$  for colloids undergoing Taylor dispersion in a pipe of width  $\chi = 0.13437$ . These are shown in Fig.8, and compared to the VACF for particles for the case of no flow. For short times both curves are well described by a simple Enskog kinetic equation (see ref [58]). Physically this is to be expected, as these kinetic processes occur on the sonic time-scale which is much faster than the flow, and so it is gratifying to see that our simulations correctly separate out this time-scale from the others. At long times the two VACFs differ. As shown in the bottom panel, the particle without flow shows the expected  $t^{-1}$  long time tail, first observed by Alder and Wainwright[68]. This tail is caused by hydrodynamic correlations that propagate through the fluid. For a finite sized pipe, we expect the tail to feel the influence of the walls at longer



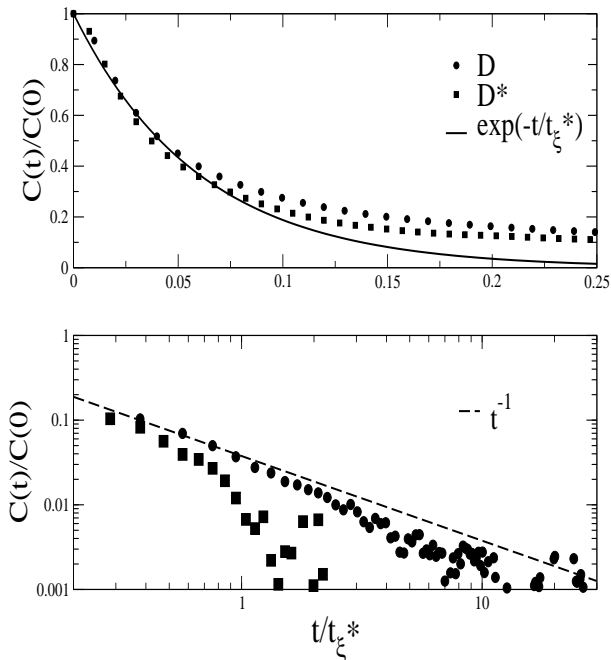


FIG. 8: Decay of the velocity autocorrelation function for particles undergoing normal (circles) and Taylor (squares) dispersion. The solid line in the top panel depicts the Enskog exponential decay. The dotted line in the bottom panel shows  $t^{-1}$  decay and serves as a guide to the eye.

times[58, 69], and some evidence of this may be visible. Nevertheless, this tail clearly differs from that of the VACF for Taylor dispersion, which shows a much more rapid non-algebraic decay. Instead it decays on a time scale comparable to  $t_{\xi^*}$ . The reason for this is most likely that the hydrodynamic correlations are washed out by the effect of the flow.

## V. SUMMARY

In summary then, we have adapted a hybrid MD-SRD technique to study colloidal discs in two dimensions undergoing flow in a narrow pipe. By carefully considering the time and length-scales involved in the problem, we were able to derive a coarse-graining method that is tractable, but still resolves the main physical properties under investigation. We measured corrections to the average flow profile, and find that the colloids move faster

than the flow when the ratio  $\chi = R/L$  increases, but that hydrodynamic wall effects also slow down the colloids when the pipes become very narrow. Finite  $\chi$  has an even bigger effect on the Taylor dispersion coefficient, decreasing its value from that expected for  $\chi = 0$ . We also measured the VACF under flow conditions, and find that this decays more rapidly than the case of no flow, most likely because the Taylor dispersion process breaks up the long-time hydrodynamic correlations.

Finally, given that we used a “telescoping down” of the hierarchy of time-scales to derive a tractable simulation scheme for the dynamics of our colloidal system, how would one “telescope up” to make experimentally relevant predictions? The first step is to cast properties of interest into dimensionless form as much as possible. From that we see, for example, that the relative decrease of Taylor dispersion depends only on the ratio  $\chi$ , and not on the absolute value of either the pipe size or the colloid radius  $R$ . Thus many different experimental colloid and pipe sizes should be describable by the same set of simulations. On the other hand, if we are interested in the long-time tails, then a more subtle analysis is needed. It appears that for colloids undergoing flow, the VACF decays on a time of the order of  $t_{\xi^*}$ , which, through Eq. (19), can be related to the Langevin time  $t_{\xi}$  and the  $Pe$  number. Again, one can rather straightforwardly estimate  $t_{\xi}$  for colloids if one knows their diffusion coefficient. However, the relative values of  $t_{\xi}$  and the diffusion time  $\tau_D$  that a colloid needs to diffuse over its own radius may be very different in the simulation than in an experiment. That means that the two time-scales in the simulation need to each be scaled differently when comparing to experiment. So in the end, to interpret a coarse-grained simulation, the best advice is to try and understand as best as possible the underlying physics.

## Acknowledgments

J.S. thanks Schlumberger Cambridge Research and IMPACT FARADAY for an EPSRC CASE studentship which supported this work. A.A.L. thanks the Royal Society (London) and J.T.P. thanks the Netherlands Organization for Scientific Research (NWO) for financial support. We thank H. Lekkerkerker for first suggesting to us that we study Taylor dispersion and R. Castillo for helpful discussions about Taylor dispersion experiments.

- 
- [1] A. A. Louis, *Phil. Trans. Roy. Soc. A* **359**, 939 (2001).
  - [2] C.N. Likos, *Physics Reports* **348**, 267 (2001).
  - [3] S. Auer and D. Frenkel, *Nature* **409**, 1020 (2001).
  - [4] E. R. Weeks *et al.*, *Science* **287**, 627 (2000).
  - [5] W. K. Kegel and A. van Blaaderen, *Science* **287**, 290 (2000).

- [6] K. N. Pham *et al.* *Science* 296, **104** (2002).
- [7] D.G.A.L. Aarts, M. Schmidt, and H.N.W. Lekkerkerker, *Science* **304**, 1944 (2004).
- [8] P. Shall, I. Cohen, D.A. Weitz and F. Spaepen, *Science* **305**, 1944 (2004).
- [9] R. P. A. Dullens and W. K. Kegel, *Phys. Rev. Lett.* **92**,

- 195702 (2004).
- [10] W. B. Russel, D. A. Saville and W. R. Showalter, *Colloidal Dispersions*, Cambridge University Press, Cambridge (1989).
- [11] J. K. G. Dhont, *An Introduction to the Dynamics of Colloids*, Elsevier, Amsterdam, (1996).
- [12] J. T. Padding and A. A. Louis, Phys. Rev. E. **74**, 031402 (2006).
- [13] A. Malevanets and R. Kapral, J. Chem. Phys. **110**, 8605 (1999).
- [14] A. Malevanets and R. Kapral, J. Chem. Phys., **112**, 7260 (2000).
- [15] R. Kapral, Adv. Chem. Phys., **140**, 89 (2008).
- [16] H. Noguchi and G. Gompper Phys. Rev. Lett. **93** (2004) 258102; *ibid* **98** 128103 (2007)
- [17] M. Hecht, J. Harting, T. Ihle, and H.J. Herrmann, Phys. Rev. E **72**, 011408 (2005).
- [18] J. T. Padding and A. A. Louis, Phys. Rev. Lett. **93**, 220601 (2004); J.T. Padding and A.A. Louis, Phys. Rev. E. **77**, 011402 (2008).
- [19] A. Wysocki *et al.*, arXiv:0810.1258
- [20] M. Ripoll *et al.*, Phys. Rev. Lett. **101**, 168302 (2008).
- [21] R. Matthews, J.M. Yeomans and A. A. Louis Phys. Rev. Lett. **102**, 088101 (2009).
- [22] G.I. Taylor: Proc. Roy. Soc. **A219** 186 (1953).
- [23] C. Van den Broeck: Physica A **112** 343 (1982).
- [24] C. Van den Broeck: Physica A **168** 677 (1990).
- [25] H. Brenner, D.A. Edwards: *Macrotransport Processes*, Butterworth-Heinemann, Boston (1993).
- [26] A. van Blaaderen, Nature **439**, 545 (2006).
- [27] E. Allahyarov, H. Löwen, A.A. Louis, and J.P. Hansen Europhys. Lett. **57**, 731 (2002); E. Allahyarov, H. Löwen, J.P. Hansen, and A.A. Louis, Phys. Rev. E. **67**, 051404 (2003).
- [28] J.P.K. Doye *et al.*, Phys. Chem. Chem. Phys. **9**, 2197 (2007).
- [29] A.A. Louis, J. Phys. Condens. Matt. **14**, 9187 (2002).
- [30] Henderson R L, Phys. Lett. A. **49**, 197 (1974).
- [31] P. Hohenberg and W. Kohn, Phys. Rev. B **136**, 864 (1964).
- [32] C.G. Gray and K.E. Gubbins, *Theory of molecular fluids*, (Oxford University Press, Oxford 1984).
- [33] J.T. Chayes and L. Chayes J. Stat. Phys. **36**, 471 (1984); J. T. Chayes, L. Chayes and E. H. Lieb, Commun. Math. Phys.; **93**, 57 (1984).
- [34] Casanova G, Dulla R J, Jonah D A, Rowlinson J S and Saville G Mol. Phys. **18** 589, (1970)
- [35] M.A. van der Hoef M A and P.A. Madden J. Chem. Phys. **111**, 1520 (1999).
- [36] M. E. Johnson, T. Head-Gordon and A.A. Louis, J. Chem. Phys. **126**, 144509 (2007).
- [37] T. Murtola, E. Falck, M. Kartunen and I. Vattulainen, J. Chem. Phys. **126**, 075101 (2007).
- [38] A.A. Louis, P.G. Bolhuis, J.P. Hansen and E.J. Meijer, Phys. Rev. Lett. **85**, 2522 (2000)
- [39] S.H.L. Klapp, D.J. Diestler, and M. Schoen, J. Phys.: Condens. Matt. **16**, 7331 (2004).
- [40] J.T. Padding and W.J. Briels, J. Chem. Phys. **115**, 2846 (2001); J.T. Padding and W.J. Briels, J. Chem. Phys. **117**, 925 (2002).
- [41] G. A. Vliegthart and P. van der Schoot, Europhys. Lett. **62**, 600 (2003).
- [42] J. Dzubiella, H. Löwen, and C.N. Likos, Phys. Rev. Lett. **91**, 248301 (2003)
- [43] P. J. Hoogerbrugge and J.M.V.A. Koelman, Europhys. Lett. **19**, 155 (1992)
- [44] P. Español and P.B. Warren, Europhys. Lett. **30**, 191 (1995).
- [45] G. A. Bird, Phys. Fluids **13**, 2676 (1970).
- [46] G.A. Bird, *Molecular Gas Dynamics and the Direct Simulation of Gas Flows* (Clarendon Press, Oxford, 1994).
- [47] A. Succi, *The Lattice Boltzmann Equation for Fluid Dynamics and Beyond*, Oxford University Press, Oxford (2001).
- [48] A.J.C. Ladd, Phys. Rev. Lett. **70**, 1339 (1993)
- [49] A.J.C. Ladd and R. Verberg, J. Stat. Phys. **104**, 1191 (2001).
- [50] M.E. Cates *et al.*, J. Phys.: Condens. Matter **16**, S3903 (2004); R. Adhikari<sup>1</sup>, K. Stratford, M. E. Cates, and A. J. Wagner, Europhys. Lett. **71**, 473 (2005); K. Stratford *et al.*, Science **309**, 2198 (2005).
- [51] V. Lobaskin and B. Dünweg, New J. of Phys. **6**, 54 (2004); V. Lobaskin, B. Dünweg, and C. Holm, J. P hys.: Condens. Matt. **16**, S4063 (2004).
- [52] F. Capuani, I. Pagonabarraga, and D. Frenkel, J. Chem. Phys. **121**, 973 (2004).
- [53] A. Chatterji and J. Horbach, J. Chem. Phys. **122**, 184903 (2005).
- [54] T. Ihle and D. M. Kroll, *Phys. Rev. E* **67**, 066705 (2003); T. Ihle and D.M. Kroll, *Phys. Rev. E* **67**, 066706 (2003).
- [55] N. Kikuchi, C. M. Pooley, J. F. Ryder, and J. M. Yeomans, J. Chem. Phys. **119**, 6388 (2003).
- [56] C.M. Pooley and J.M. Yeomans, J. Phys. Chem. B **109**, 6505 (2005).
- [57] J.T. Padding, A. Wysocki, H. Löwen, and A.A. Louis, J. Phys.: Condens. Matt. **17**, S3393 (2005).
- [58] J. Sané, J.T. Padding and A.A. Louis, arXiv:0812.3618
- [59] J. Happel and H. Brenner, *Low Reynolds Number Hydrodynamics* (Springer, 1973).
- [60] T.M Squires, S.R. Quake: *Microfluidics: Fluid Physics at the Nanoliter Scale*, (2004)
- [61] R.F. Probstein: *Physicochemical Hydrodynamics*, Wiley and Sons (1994).
- [62] G.I Taylor: Proc. Roy. Soc. **A225** 473 (1954).
- [63] Jimaan Sané PhD Thesis. (2008)
- [64] R. Aris: Proc. Roy. Soc. **A235** 67 (1956).
- [65] R. Castillo, C. Graza and S. Ramos, J. Phys. Chem. **98**, 4188 (1994).
- [66] A.J. McHugh: *Hydrodynamic Chromatography. In 'Size Exclusion Chromatography'* B.J. Hunt and S.R. Holding. New York: Chapman and Hall (1989).
- [67] H. Brenner, L.J. Gaydos: J. Coll and Interf. Sci. **58** 313 (1976).
- [68] B.J. Alder and T.E. Wainwright, *Phys. Rev. A* **1**, 18 (1970).
- [69] M.H.J. Hagen, I. Pagonabarraga, C.P. Lowe, D. Frenkel: Phys. Rev. Lett **78**, 3785 (1997).